ETH zürich

ETH Library

Soft Gripper with Adjustable Microspines for Adhering to Tree Branches

Conference Paper

Author(s):
Kirchgeorg, Steffen; Benist, Bram; Mintchev, Stefano

Publication date:
2022

Permanent link:
https://doi.org/10.3929/ethz-b-000574190

Rights / license:
In Copyright - Non-Commercial Use Permitted

Originally published in:
Lecture Notes in Networks and Systems 530, https://doi.org/10.1007/978-3-031-15226-9_9

Funding acknowledgement:
186865 - CYbER - CanopY Exploration Robots (SNF)

This page was generated automatically upon download from the ETH Zurich Research Collection.
For more information, please consult the Terms of use.

Soft gripper with adjustable microspines for adhering to tree branches

Steffen Kirchgeorg[1], Bram Benist[2], and Stefano Mintchev[1]

[1] ETH Zürich, 8092 Zürich, Switzerland and
WSL, 8903 Birmensdorf, Switzerland
skirchgeorg@ethz.ch,
[2] TU Delft, 2628 CD Delft, Netherlands

Abstract. Labour and resource intensive data collection methods drive the use of unmanned aerial vehicles in the field of environmental monitoring. UAV supported sensor deployment in forests can improve localized and continuous monitoring. To advance this field, we present a two fingered gripper with spines integrated on three phalanxes. The softness of the fingers combined with compliantly-supported microspines integrated into adjustable microspine-clusters allow the gripper to wrap and adhere to tree branches. With a differential drive actuation, microspine cluster adjustability as well as load-sharing between spine clusters is achieved. We characterize the bending behaviour of the soft fingers that adapt to curved and irregular objects. We show that the implementation of compliantly-supported and adjustable microspine-clusters increase holding force and that load-sharing between spine clusters is achieved with the differential drive actuation. The demonstration of UAV perching on a tree branch with the gripper shows that sensor deployment in these environments can be achieved.

Keywords: Mechanism design, Grasping, Gripping, Adhesion, Microspines

1 Introduction

Arboreal ecosystems gained fast growing scientific interest in the last decades as they are essential for global as well as local carbon, gas and water cycles [1]. The local, near-surface microclimates exhibited in these ecosystems depend on the global climate and vice-versa, resulting in an interdependence and complex relationship [2]. To date, monitoring is achieved with instantaneous manual sampling or deployment of sensors by either experienced climbers or on expensive fixed structures, such as canopy cranes [1]. With limited and difficult access, gaps remain in the localized and continuous sampling, but first robotic approaches for acquiring data have been proposed. Climbing robots that adhere and move on the tree structure have low power consumption [3],but handling complex manoeuvres, e.g. transitioning from the trunk to a branch, reliably remains an open research challenge [1]. Compared to climbing robots, aerial vehicles can easily reach forests and become of greater interest for continuous sampling and monitoring within canopies. UAVs have already demonstrated sensor deployment [4]

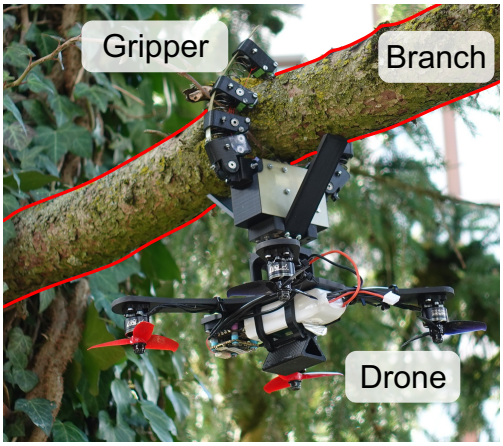

Fig. 1. A UAV using the soft gripper with microspines for perching on a tree branch.

or may serve as a sensor platform themselves by resting and perching on tree branches [5] . For either, the challenges lie in adhering with a sensor or the robot to the environment. Despite good performance on flat and artificial surfaces, wet- [6], dry- [7] and electro-adhesion [8] cannot yet handle the irregular bark of trees. Other approaches include using high-friction material [9] or grasping the whole object [10]. The most promising and employed approaches for adhering to tree barks are penetrating needles and microspines. Former can grasp and attach to branches in different orientations [11], but the large force required to penetrate the bark will push a gripper away from the surface unless it is kept in position by an external force during the attachment process. Microspines, on the other hand, have been demonstrated to adhere to small asperities on a variety of rough surfaces with low pressing or actuation force. [12, 13] present rock grippers based on compliantly-supported microspines integrated into movable spine-clusters. This hierarchical design obtained by combining spine and cluster level adjustability allow the spines to travel along the surface and maximize the chance to find asperities. The grippers perform well on low curvature surfaces, but larger curvature obstacles pose a problem as the gripper bodies have limited [12] or no compliance [13] to adjust to curved objects. By taking advantage of a soft body, [14] developed a grapple that can conform to irregular overhanging surfaces, but does not include adjustability of the spines.

By taking inspiration from previous works, we combined a soft-robotics approach with compliantly-supported microspines integrated into microspine-clusters to develop a novel gripping strategy and a prototype gripper for curved rough surfaces as shown in Fig. 1. Our strategy exploits two soft fingers that adapt to curved and irregular objects, and two complementary approaches that increase spine engagement with the target surface by allowing the translation of both individual and clusters of spines. By granting each spine more freedom to move, the chance a spine engages is maximized. A differential drive actuation controls the closing of the fingers, enables spine cluster translation and load-sharing between clusters, such that the holding force, or payload, of the gripper is increased.

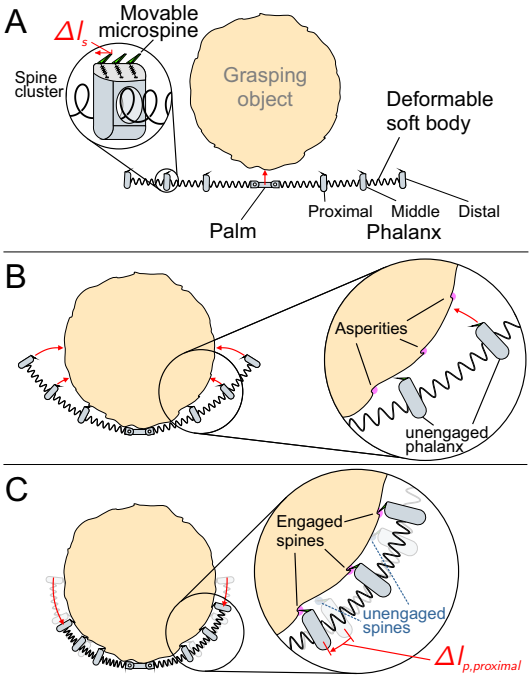

Fig. 2. Illustration of the gripping strategy. **A** The gripper uses two fingers with three phalanxes with multiple compliantly supported microspines (zoom-in) that are compliantly integrated (zoom-in), which enables them to move and adjust by Δl_s to find asperities. **B** Actuation of the fingers cause curling and brings phalanxes close to the grasping object. The spines start contacting the surface and look for asperities. **C** After full contact with the object, the fingers contract and the phalanxes travel along the surface, enabling the microspines to find and engage with asperities. Each finger can move independent of the other phalanxes within a small range by Δl_p.

In the following section, we detail the developed gripping strategy and subsequently describe how it is translated into a mechanical design of a gripper in section 3. We then characterize the gripper by analyzing its soft behaviour and the spine cluster and spine level adjustability as well as load-sharing in section 4. Finally, we demonstrate the gripper on tree barks and integrat it on a UAV for perching on tree branches, simulating a possible sensor deployment scenario.

2 Gripping strategy

Tree stems and branches are usually circular, but may have irregular features such as bumps and fissures due to their barks. Depending on the tree species, surface roughness can span from very smooth to rough. Microspines have shown strong carrying capacity and large surface versatility by holding on to small asperities in the surface [15]. However, they need to actively find suitable asperities, whose amount, depth and strength greatly depends on the material and surface roughness. Two failure mechanisms have been identified for microspines: slipping from an asperity and overload [16]. Overload causes damage either to the spine or the asperity, such that adhesion is no longer possible.

Our gripping strategy therefore aims to enable spines to find suitable asperities, thus avoiding slippage, as well as avoid overload by load-sharing between spines. This gripping strategy is illustrated in Fig. 2 and based on a palm-finger structure that exploits four principles: (i) A soft behaviour gives the fingers the ability to adjust to irregular shaped surfaces (Fig. 2B and C). Furthermore, mi-

crospines are employed in a hierarchical fashion with (ii) adjustability on the spine cluster-level, i.e. the proximal, middle and distal phalanxes and (iii) individual spine-level compliance. (iv) Load-sharing complements the strategy by allowing the load to be distributed among engaged spines. The two mechanisms for adjustability of the spines increase their engagement chances by giving the microspines two complementary degrees of freedom to find, adhere and continue adhering to asperities. By complementing them with a load-sharing ability (section 3.2), the second failure mode, spine overload, can be reduced.

2.1 Spine cluster adjustability

On a spine cluster-level, each phalanx is connected through a soft connection that enables the fingers to not only curl around curved objects (Fig. 2B), but also to contract upon actuation (Fig. 2C) and thus allows the phalanxes and their spine clusters to travel along the surface of the object (Fig. 2C zoom-in). In this way, a phalanx with unengaged spines (Fig. 2C zoom-in) can translate by Δl_p and find suitable asperities on the target surface. The soft connection allows each phalanx to translate, within some bounds, regardless of the other phalanxes such that the engagement of spines on one phalanx does not hinder further translation and engagement of the other spine clusters.

2.2 Spine-level adjustability

On a spine-level (Fig. 2A zoom-in), adjustability is achieved by compliantly integrating the microspines in the phalanxes. Each microspine within a spine cluster can therefore travel slightly by Δl_s with respect to the phalanx to adjust to minor changes in the surface. Therefore, multiple spines within a spine cluster can engage with different asperities.

3 System description

In this section, we describe how the aforementioned gripping strategy with hierarchical compliance for both cluster and individual spine adjustability is translated into a mechanical design, and how system actuation and load-sharing is achieved.

3.1 Mechanical Design

The gripper consists of a palm and two soft fingers as illustrated in Fig. 3A. Three phalanxes with five microspines each are distributed along the finger length. A spring and a fiberglass reinforcement are used as a backbone for each finger. The spring allows the finger to bend in order to adjust to curved objects while the flat fiberglass reinforcement limits torsion within the finger. With this simple, yet effective design we achieve the soft behaviour, which forms the basis for our gripping strategy. The spring-based design was furthermore chosen to comply with the strategies' second principle: spine-cluster adjustability. By employing a spring, the phalanxes can travel along the spring's length through compression. The 3D printed phalanxes (Fig. 3B) are fixed in place on the spring by a blocking fiberglass sheet, but can slide on the fiberglass reinforcement, which

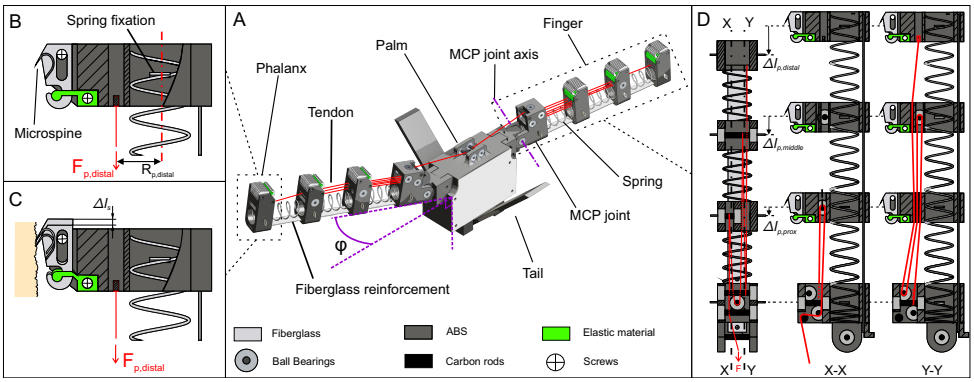

Fig. 3. Mechanical design and tendon routing: **A** Overall design with a palm and two fingers that can curl as well as rotate around the MCP joint axis. **B** Each phalanx has five microspines integrated with an elastic material such that **C** multiple spines can engage with a surface as each spine can translate by Δl_s. **D** Tendon routing allows for a differential drive actuation such that each phalanx can travel regardless of the other two by Δl_p.

therefore only limits torsion. Each phalanx represents a spine cluster made up of five microspines and by compression of the spring each cluster or phalanx translates (Fig. 3D). The phalanxes separate the spring sections such that each can compress independently. However, this requires a specific differential drive actuation with tendons, as described in detail in the next section. To ensure the principle of spine-level adjustability, the microspines are compliantly integrated in the phalanxes. Each spine is attached through an elastic material (3D printed Ninjaflex), which acts as a spring, to the phalanx. The motion of the spine is limited by a screw and a slot in the vertical direction (Fig. 3B and C). The five spines within a cluster can individually translate with respect to the phalanx and their neighbouring spines by a distance Δl_s. Once a spine engages with an asperity, it can translate with respect to the phalanx and remain attached to the found asperity while other spines continue translating with the phalanx. Two engaged, but vertically shifted spines in a single phalanx are shown in Fig. 3C.

Apart from the design considerations for the main working principles, slight adaptations were made to improve performance. A joint, much like the metacarpophalangeal (MCP) joint between the human finger and hand, is added between finger and palm to allow the finger to rotate and thus quickly adapt to the object before bending its finger. The fingers are also slightly rotated by φ to avoid colliding with each other when encircling smaller objects. Additionally, stabilizing tails are added to the palm to counteract a pitch-back moment that arises on inclined surfaces. As the center of mass (COM) is at a certain distance from the surface, a pitch-back moment occurs on inclined surfaces. Animals counteract it with tails [17], which is why two 3D printed tails are added whose shape and size may be adapted to the target application and surface.

3.2 Differential drive actuation and load-sharing

The fingers are actuated through tendons and a differential drive actuation, as shown in Fig. 3D is employed to ensure that phalanxes can travel independently. By passing the tendon from one phalanx back to the MCP joint before passing it to the next phalanx, the following forces F_p are applied:

$$\begin{aligned} F_{p,proximal} &= 2F\ , \quad & R_{p,proximal} &= 9\,\text{mm}\ , \\ F_{p,middle} &= 2F\ , & R_{p,middle} &= 8\,\text{mm}\ , \\ F_{p,distal} &= F\ , & R_{p,distal} &= 9\,\text{mm}\ , \end{aligned} \tag{1}$$

with F as the actuation force and R_p the moment arm between applied phalanx force F_p and the springs' central axis (Fig. 3B). The applied moments F_pR_p result in bending of the finger, with bending starting from the proximal phalanx and moving towards distal phalanx due to decreasing moments. This was chosen such that the gripper adjust to the surface's curvature from the proximal phalanx, as a bending initiated from the distal phalanx would result in a curvature smaller than that of the object. Once bending is restricted, an increase in actuation force compresses the spring and results in travel of the phalanxes. As each spring section before a phalanx is free to compress or even elongate, each phalanxes can travel independently even though their motion is constrained by the other phalanxes.

The tendon routing shown in Fig. 3D also enables load-sharing among spine clusters. An engaged spine restricts movement of the phalanx as it counteracts the applied force F_p on the phalanx. While the phalanx will remain in place, other phalanxes continue to translate until their spines engage to counteract F_p on their respective phalanx. Either the spines or the compression force of the spring will counteract F_p (applied by actuation force F according to eq. (1)) and once this is achieved for all phalanxes, the gripper stops bending and translating. Any increase in F, i.e. a payload, is transferred onto the phalanxes and then spines and thus shared between the engaged spines according to the previously presented distribution in eq. (1).

The tendons are routed to a brushed DC motor in the palm via the MCP joint and when the tendons are actuated, the fingers will first rotate around the MCP joints as it's the path of least resistance. Once a phalanx gets in contact with an object, the motion is restricted and the finger starts bending. Lastly, the spring compresses until the spines are engaged and the actuation force is balanced out. In order to reduce friction forces arising from tendon redirection, the tendons are routed via carbon rods mounted in ball bearings. This eventually reduces the actuation force of the system.

For the control of the motor, an Arduino board (TinyDuino) and a battery are housed in the palm. The motor is connected through a worm-gear to the tendon spool, which automatically locks the position of the gripper when no power is supplied. The power of the motor can be adjusted such that it stalls when reaching a chosen activation force. The Arduino and thus the motor can be controlled remotely via Bluetooth Low Energy (BLE) to wind and unwind the tendons.

All in all, the mechanical design and differential drive actuation ensures that the amount of engaged microspines is maximized by allowing each spine to move independently, even when a spine within the same phalanx or within the same finger obtains a holding force by engaging with an asperity.

4 Results

The gripping strategy and derived mechanical design relies on fingers with a soft body and a maximization of spine engagement through hierarchical adjustability of spines and spine clusters. We first characterize the soft bending behaviour of the finger and compare it to model data in section 4.1. We then prove that adjustability on the spine-level, section 4.2, and cluster-level combined with load-sharing, section 4.3, enable larger holding forces. Finally, we perform payload tests indoors for different sandpaper roughnesses in section 4.4.

4.1 Characterization of finger curvature

The fingers need to adjust to the curvature of the gripping object. The force needed to bend the spring to achieve a certain curvature, i.e. a desired grasp diameter, was first modeled and subsequently experimentally verified. Here, we neglect the fiberglass reinforcement that prevents torsion due to its low bending stiffness. According to [18], the bending angle θ of a spring can be expressed as:

$$\theta = n\pi M R_s \left(\frac{1}{EI_a} + \frac{1}{GI_p} \right) \tag{2}$$

with n the amount of spirals in the spring, M the moment applied to the spring, R_s the radius of the spring, E the elastic modulus of the spring material, I_a the area moment of inertia, I_p torsional moment of inertia, and G the shear modulus. As the finger is segmented into three discrete parts, at which each end a phalanx is attached, we first compute the bending angles θ based on the moments M applied with the forces F_p and moment arms R_p according to eq. 1. The bending angles for proximal, middle and distal phalanx are then converted to a diameter of curvature with:

$$D = \frac{C}{\pi} \ , \quad C = \frac{360^\circ}{\theta_{proximal} + \theta_{middle} + \theta_{distal}} (L - \Delta H) \ , \tag{3}$$

given L the spring length without any compression and ΔH the compression length. The diameter to which the spring adjusts to, given an actuation force F and a spring constant k, is then computed as:

$$D = \frac{360^\circ}{\theta_{proximal} + \theta_{middle} + \theta_{distal}} \frac{(L - \frac{F}{K})}{\pi} \ . \tag{4}$$

Fig. 4 shows the obtained model data as well as the experimental data acquired by applying a force F to a single finger and conforming to a diameter D with the setup shown in Fig. 4. While the experimental and model data share the same trend, a small difference in force is noticeable. Even though the mechanical design was optimized and ball bearings with carbon rods used to reduce friction, the tendon routing still resulted in noticeable friction that has to be overcome. The model does not account for friction, therefore predicting a smaller forces.

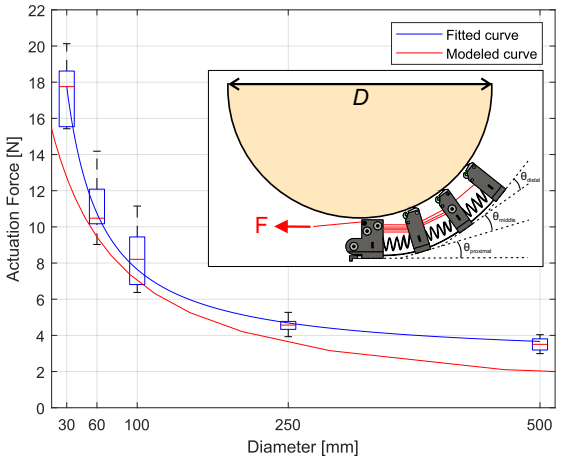

Fig. 4. Model and experimental data for the force required to bend a finger to achieve different diameters. Experimental data is based on ten measurements per diameter. Inset shows experimental setup and the angles θ required to calculate model data.

4.2 Spine-level adjustability

We integrated spines in each phalanx with a compliant 3D-printed material such that travel between adjacent spines is permitted. In order to validate that this enables higher holding forces, we compared the compliantly integrated spines to a rigid baseline. On a flat 80-grit sandpaper surface, we tested a finger with a single distal phalanx with five spines. The phalanx was engaged on the sandpaper using an actuation force of 10 N. Then, the sandpaper was pulled off in the opposite direction to simulate a payload. This force was measured and results for ten trials are shown in Fig. 5A. While the maximum holding force does not vary significantly, the compliantly integrated spines improve the mean holding force and reduce statistical variability compared to the baseline. In other words, the probability of all five spines finding an asperity is higher for the movable spines. This is also supported by the Wilcoxon Signed Rank Test with a value of $p \leq 0.05$, meaning that the compliant spines behave statistically significantly different from the rigid spines.

4.3 Spine cluster adjustability and load sharing

In order to achieve independent translation of each phalanx, a differential drive that distributes the actuation force to each phalanx according to eq. 1. Thus, each phalanx can independently move, find asperities and halt translation to stay attached to the asperities. To ensure that the differential drive system achieves this behaviour, we performed experiments to compare the pulley-actuated system with two baselines, as shown in the insets in Fig. 5B. The first baseline is a finger with fixed phalanxes, where all phalanxes are constrained to move together and no independent movement is allowed. The second baseline is a distal phalanx actuated system, but the spring sections and thus the phalanxes can compress differently. In each experiment, the finger was engaged with a flat 80-grit sandpaper with an actuation force of 3.3 N for the fixed phalanx baseline and 10 N for the other experiments. The actuation force was reduced for

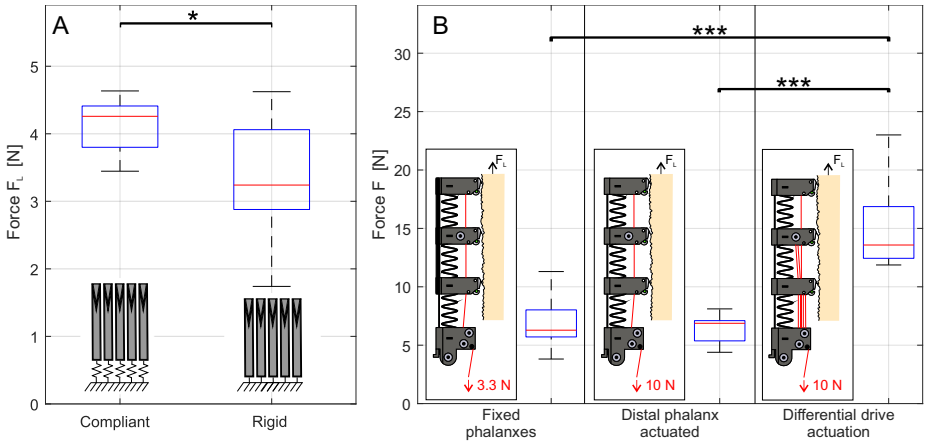

Fig. 5. Maximum holding force experiments on 80-grit sandpaper. **A** Force a phalanx with 5 compliant or 5 rigid spines can achieve with an activation force of 10 N before failure. **B** Holding force the fixed phalanxes, distal phalanx actuated and differential drive actuated system can achieve. Ten measurements were made each. Single and triple star indicate a probability of 5% and 0.1% of one the final systems performing worse than the baselines.

the fixed phalanx experiment, as only the first spring element could compress. Subsequently, the sandpaper was pulled in the opposite direction to simulate a payload. The maximum force until failure for each system was recorded and evaluated for 10 measurements.

When comparing the fixed phalanx system to the final design, a twofold increase in holding force can be observed. As all phalanxes move together, less spines engage and even if multiple spines engage, the force does not seem to get distributed among them. The second baseline has a similar holding force as the first baseline. While all phalanxes can move, only the distal phalanx is actively actuated and therefore properly engages in the experiment. It becomes apparent that not only individual movement of the phalanxes must be allowed, but also each phalanx has to be actuated directly and the load preferably shared among engaged spines as mentioned in section 3.2. Therefore, the differential drive actuated system engages more spines as well as shares the load between engaged spines, allowing for a twofold increase over the baselines. The Wilcoxon Signed Rank Tests also suggests that the probability of the differential drive system performing worse than the other baselines is less than 0.1%.

4.4 Payload tests

We have performed tests with a payload of 1 kg for different surface roughnesses. The gripper was pressed vertically against cylindrical surfaces of different diameter as shown in the inset in Table 1. The tests were carried out with an activation force of 25 N split across two fingers. The successful to total attempts are summarized in Table 1. K60-K120 describe the sandpaper rating, with K60 being the roughest and K120 the finest sandpaper tested. The gripper performs

Table 1. Indoor tests with a payload of 1 kg for different diameters and surface roughnesses. Low K-values refer to rough, while large K-values refer to smooth surfaces. Inset shows experpimental setup.

	Diameter [mm]		
Roughness	30	60	100
K60	5/5	5/5	4/5
K80	5/5	5/5	0/5
K100	5/5	5/5	0/5
K120	4/5	3/5	0/5

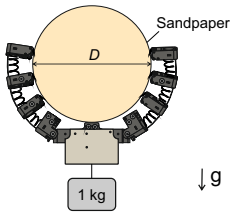

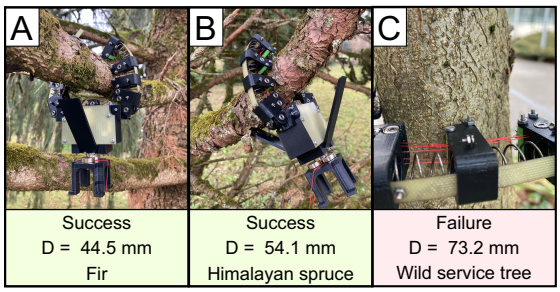

Fig. 6. Tests on different tree species with two successful and one failed engagement.

well for smaller diameters of 30 to 60 mm for all tested roughnesses. For a target with a 100 mm diameter, the gripper performs well for the roughest sandpaper but quickly fails for finer sandpaper. In this case, the gripper cannot exploit clamping as it spans less than half of the circumference of the obstacle. Nevertheless, with a rough sandpaper (K60) the gripper can still acquire normal forces from engaging with the asperities. For finer sandpapers, however, it becomes harder to engage and obtain holding forces from the small asperities. The microspines can easily slip from the smaller, shallower and rounded asperities in the fine sandpaper, causing the system to fail.

5 Demonstration

We have performed outdoor tests on several trees with a payload of 1 kg as well as integrated the gripper on a UAV for perching. For the former, the gripper was pushed manually against the tree with its palm and the fingers were subsequently actuated. After reaching the maximum actuation force, the finger actuation stops and the manual support was released, such that the payload of 1 kg was fully transferred onto the gripper. A selection of two successful and one failed example is shown in Fig. 6. For the successful attempts, Fig. 6A and B, the gripper properly encircled and adjusted to the tree branch curvature. All phalanxes are in contact with the tree branch, thus maximizing the amount of microspines that can engage with the surface. It also becomes apparent that the left tail counteracts the pitch-back moment in Fig. 6B, stabilizing the gripper. Fig. 6C shows a more vertically oriented tree branch of the wild service tree,

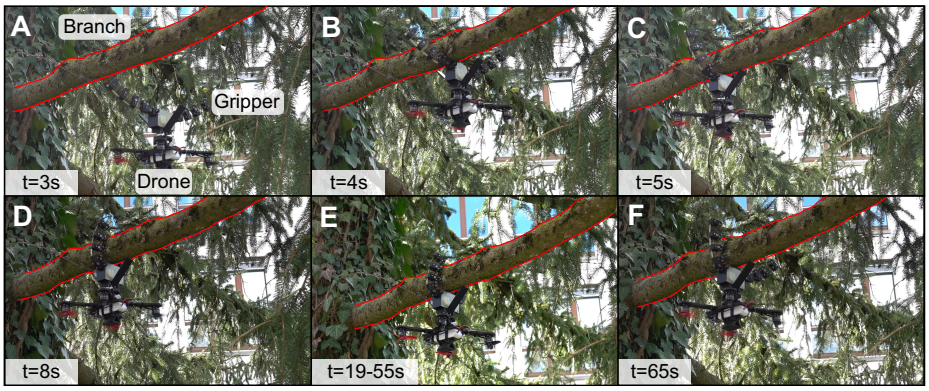

Fig. 7. Sequence of the UAV perching on a tree branch. A full clip is available: https://youtu.be/pTffRYXPBwQ

for which the gripping failed. Adhesion is more challenging due to the smoother surface and larger diameter compared to the himalayan spruce and the fir. Furthermore, the more vertical orientation of the branch may cause shear forces on the spines, which they do not handle well. Additionally, the pitch-back moment is large and the currently employed tail could not fully counteract it. A longer tail, or a three finger design would improve the gripping in this situation.

We integrated the gripper on the top of a UAV and demonstrate teleoperated perching of the system on a tree branch in Fig. 7. The UAV approaches the branch (Fig. 7A), aligns with it and makes contact with the palm (Fig. 7B) before actuating the gripper (Fig. 7C). The gripper closes and encircles the object, thus engaging the microspines for adhesion (Fig. 7E). The motors were fully turned off for maximum power saving. Afterwards, the gripper actuation was reversed and it disengaged from the branch, allowing the UAV to fly away as visible in Fig. 7F. The demonstration was achieved completely teleoperated without an additional control strategy. Once the gripper started closing around the branch, it stabilized the drone and eased teleoperation. However, it is necessary for the drone to maintain a stable hover for several seconds prior to gripper engagement. The demonstration is also comparable to sensor deployment as the gripper could simply be detached from the UAV after engagement.

6 Conclusion

A gripping strategy maximizing microspine engagement with adjustability on a spine and spine cluster level has been presented and translated into a mechanical design of a soft bodied gripper to grasp circular objects. By providing the microspines with two complementary degrees of adjustability, we improved spine engagement. We showed that the individual translation of spine clusters through a differential drive actuation coupled with the soft body increases the holding force of the mechanism two- to threefold. Furthermore, compliantly integrated spines within a spine cluster allow for independent micro adjustment of the microspines to asperities, further maximizing engagement and thus holding force.

The designed gripper successfuly attached to a variety of controlled surface roughnesses and diameters as well as on tree barks outdoors. An integration of the gripper on a drone and perching on a branch showed that the use within a dynamically moving system is feasible. For larger diameters with low surface roughness, the addition of penetrating needles beside the microspines may improve adhesion of the system. Furthermore, a continuously soft finger from silicone could simplify the mechanical design and reduce actuation force, while also allowing the integration of microspines along the full body of the finger. A study on finger number and finger orientation for the desired application could also enhance capabilities.

With the proposed strategy and design, we hope to advance towards more versatile and reliable gripping solutions for robots in natural environments. Such solutions will improve and allow scaling of microclimate and ecosystem monitoring tasks in the future.

References

[1] Cannon, C.H., Borchetta, C., Anderson, D.L., et al.: Extending our scientific reach in arboreal ecosystems for research and management. Frontiers in Forests and Global Change p. 160 (2021)
[2] Nakamura, A., Kitching, R.L., Cao, M., et al.: Forests and their canopies: Achievements and horizons in canopy science. Trends in Ecology & Evolution 32(6), 438–451 (2017)
[3] Tavakoli, M., Viegas, C.: Bio-inspired climbing robots. In: Biomimetic Technologies, pp. 301–320. Elsevier (2015)
[4] Farinha, A., Zufferey, R., Zheng, P., et al.: Unmanned aerial sensor placement for cluttered environments. IEEE Robotics and Automation Letters 5(4), 6623–6630 (2020)
[5] Hang, K., Lyu, X., Song, H., et al.: Perching and resting—a paradigm for uav maneuvering with modularized landing gears. Science Robotics 4(28), eaau6637 (2019)
[6] Langowski, J.K., Dodou, D., van Assenbergh, P., van Leeuwen, J.L.: Design of tree-frog-inspired adhesives. Integrative and comparative biology 60(4), 906–918 (2020)
[7] Hawkes, E.W., Christensen, D.L., Cutkosky, M.R.: Vertical dry adhesive climbing with a 100× bodyweight payload. Proceedings - IEEE International Conference on Robotics and Automation 2015-June(June), 3762–3769 (2015)
[8] Prahlad, H., Pelrine, R., Stanford, S., et al.: Electroadhesive robots - Wall climbing robots enabled by a novel, robust, and electrically controllable adhesion technology. Proceedings - IEEE International Conference on Robotics and Automation pp. 3028–3033 (2008)
[9] Kirchgeorg, S., Mintchev, S.: Hedgehog: Drone perching on tree branches with high-friction origami spines. IEEE Robotics and Automation Letters 7(1), 602–609 (2021)
[10] Zhang, H., Sun, J., Zhao, J.: Compliant bistable gripper for aerial perching and grasping. In: 2019 International Conference on Robotics and Automation (ICRA). pp. 1248–1253. IEEE (2019)
[11] Xue, K., Qian, H., Sun, Z.: Design of An Adaptive Mini Gripper for Climbing Robots. ICARM 2018 - 2018 3rd International Conference on Advanced Robotics and Mechatronics pp. 618–623 (2019)
[12] Parness, A., Frost, M., Thatte, N., et al.: Gravity-independent rock-climbing robot and a sample acquisition tool with microspine grippers. Journal of Field Robotics 30(6), 897–915 (nov 2013)
[13] Wang, S., Jiang, H., Cutkosky, M.R.: A palm for a rock climbing robot based on dense arrays of micro-spines. IEEE International Conference on Intelligent Robots and Systems 2016-Novem, 52–59 (2016)
[14] Nguyen, H.N., Siddall, R., Stephens, B., et al.: A passively adaptive microspine grapple for robust, controllable perching. RoboSoft 2019 - 2019 IEEE International Conference on Soft Robotics pp. 80–87 (2019)
[15] Provancher, W.R., Clark, J.E., Geisler, B., Cutkosky, M.R.: Towards penetration-based clawed climbing. In: Climbing and walking robots, pp. 961–970. Springer (2005)
[16] Jeffries, L., Lentink, D.: Design Principles and Function of Mechanical Fasteners in Nature and Technology. Applied Mechanics Reviews 72(5) (sep 2020)
[17] Haynes, G.C., Khripiny, A., Lynch, G., et al.: Rapid pole climbing with a quadrupedal robot. Proceedings - IEEE International Conference on Robotics and Automation 2009, 2767–2772 (2009)
[18] Yan, J., Shi, P., Xu, Z., Zhao, J.: Design and kinematics of cable-driven soft module coupled with spring. IEEE International Conference on Robotics and Biomimetics, ROBIO 2019 (July 2021), 2195–2200 (2019)